行政院國家科學委員會補助專題研究計畫 ■ 成 果 報 告 □期中進度報告

考慮結構-土壤-結構互制分析高科技廠房結構之微振動行為及地盤之波傳行為

計畫類別：■ 個別型計畫　　□ 整合型計畫

計畫編號：NSC 96－2221－E－009－082－

執行期間：　96 年 08 月 01 日至　97 年 07 月 31 日

計畫主持人：劉俊秀

共同主持人：

計畫參與人員：

成果報告類型(依經費核定清單規定繳交)：■精簡報告　□完整報告

本成果報告包括以下應繳交之附件：

■赴國外出差或研習心得報告一份

□赴大陸地區出差或研習心得報告一份

□出席國際學術會議心得報告及發表之論文各一份

□國際合作研究計畫國外研究報告書一份

處理方式：除產學合作研究計畫、提升產業技術及人才培育研究計畫、列管計畫及下列情形者外，得立即公開查詢

□涉及專利或其他智慧財產權，□一年□二年後可公開查詢

執行單位：

中　華　民　國　　97 年　　09 月　　14 日

摘要

本研究將發展一種求得彈性半空間上任何位置振動之方法。此振動之振動源為彈性半空間上一剛性圓基礎受一簡諧振動力。在這方法中，圓柱座標系統之三維波動方程式的解析解將被利用。因此求得在彈性半空間上任何一點之振動可由對波數k積分之半無限積分式(k從0積到∞)表示。但在數值積分上，吾人只可能從0積分到某一積分上限k_u。而此積分上限必須足夠大以求得精確之結果。能夠以積分上限代替無限大是因積分式中之積分項是以$1/k^2$衰減。經由本研究顯示，積分上k_u之選取與非因次化頻率，振動源與振動位置間之非因次化距離及彈性半空間之阻尼比有關。同時本研究亦發現在某一方向之振動量並非單純隨與振動源之距離變大而減少。此種現象乃因表面波影響之現象。本研究同時將探討阻尼比對振動衰減之影響。本研究亦證明本研究所發展之方法有效。

Abstract

The paper presents a systematic procedure to calculate the vibration at any specific location on a half-space medium due to harmonic vibrations of a circular rigid plate on the medium. In the procedure, the analytic solutions of 3D wave equations in cylindrical coordinates are employed. The vibration at any specific location on half-space medium is obtained analytically by a semi- infinite integration with respect to wave number k from 0 to ∞. However, the numerical integration will be only performed up to a certain upper limit k_u instead of ∞. InThe paper presents a systematic procedure to calculate the vibration at any specific location on a half-space medium due to harmonic vibrations of a circular rigid plate on the medium. In the procedure, the analytic solutions of 3D wave equations in cylindrical coordinates are employed. The vibration at any specific location on half-space medium is obtained analytically by a semi- infinite integration with respect to wave number k from 0 to ∞. However, the numerical integration will be only performed up to a certain upper limit k_u instead of ∞. In order to keep the accuracy, the upper limit k_u must be large enough. The choosing of the integration upper limit k_u is dependent upon the factors of nondimensional vibration frequency, nondimensional distance between vibration source and receiving location and material damping of the medium. From the numerical results, one finds that the vibrations may not attenuate monotonically along the distance from source. This is due to the phenomenon of Rayleigh surface wave. The influence of hysteretic damping of medium on the attenuation of vibration is also investigated. Some numerical results will be shown and discussed. Comments on the presented method and numerical results will be given, and the presented scheme is proved to be effective and efficient for accurately calculating the vibration induced by harmonic loadings applied at rigid circular plate.

k_u k 以 order to keep the accuracy, the upper limit k_u must be large enough. The choosing of the integration upper limit k_u is dependent upon the factors of nondimensional vibration frequency, nondimensional distance between vibration source and receiving location and material damping of the medium. From the numerical results, one finds that the vibrations may not attenuate monotonically along the distance from source. This is due to the phenomenon of Rayleigh surface wave. The influence of

hysteretic damping of medium on the attenuation of vibration is also investigated. Some numerical results will be shown and discussed. Comments on the presented method and numerical results will be given, and the presented scheme is proved to be effective and efficient for accurately calculating the vibration induced by harmonic loadings applied at rigid circular plate.

Introduction

Environmental vibrations near vibration source will affect the performance of high precision equipments or hi-tech production machines; e.q. optical tools used by microelectronics industry. Therefore how to specify the allowance of ground vibration for those hi-tech production equipments and how to evaluate the ground vibration due to a specific vibration source have become important issues for design and construction of hi-tech production plants.

In response to the first problem, Gordon and Dresner [1] have proposed the generic vibration criterion curves for different vibration sensitive equipments. From these curves, one can find the allowable ground vibration is getting smaller as the production requirement is getting stricter. To address the second problem Sheng et al [2] and Krylov [3] employed Euler beam theory to model whole track including rails, steepers and ballast, and Kaynia et al [4], Takemiya and Bian [5,6] proposed a more sophisticate analysis model, which takes dynamic interaction into account, to evaluate the ground vibration induced by passing train. To reduce the ground vibrations near track, open or in-fill trenchs are usually recommended. Ahmad and Al-Hussaini [7] and Dasgupta et al [8] have given some theoretical studies. Moreover, if the track is elevated on bridges, the ground vibration due to the excitations by bridge abutments will produce more serious problem to the hi-tech production tools. Takemiya [9] designed a wave impeding barrier of honeycomb piles to reduce the ground vibrations near bridge abutments. Therefore, the calculation of ground vibrations induced by vibration of bridge foundation due to passage of high speed train is very important for high precision production equipments nearby.

All above mentioned methods, finite element or boundary element based methods are employed to model half-space medium. Regarding the analytical approach to evaluate the ground vibration due to specific sources, Miller and Pursey [10] have calculated the energy flux of compressional, shear and Rayleigh waves in the far-field of a semi-infinite medium generated by vertical harmonic vibration of circular plate. Also from the practical point of view, Woods and Jedele[11] collected some observation data and deduced these data into a simple formula expressing the attenuation relationship of vibration in terms of distance and soil damping.

The paper will present an analytical procedure to calculate the vibration at any location

of half-space medium due to harmonic vibration of a rigid circular plate. The components of harmonic vibration of the plate are torsional, vertical, horizontal and rocking motions. To solve the problem of wave propagation in half-space medium, Liou [12] have developed a technique to decompose the applied tractions induced by vibrations of plate. These decomposed tractions will be easily fitted into the analytic solutions of three dimensional wave equations in cylindrical coordinates. This technique was employed to generate the impedance functions for circular plate on half-space medium by
Liou et al [13]. The presented procedure in the paper will extend the work of Reference 13 to generate the vibration at any location on half-space medium due to a harmonic loading applied at a rigid circular plate.

In order to simulate the distribution of interaction tractions between rigid plate and surrounding medium, piecewise linear distribution in r-direction of cylindrical coordinates is assumed. Based on this assumption, the impedance functions for the plate can be obtained by enforcing compatibility condition, using variational principal and reciprocal theorem. The vibration at any specific location on half-space medium can also be calculated for the cases of applying harmonic loadings at the plate.

Numerical results for a rigid circular plate subjected to torsional, vertical, horizontal and rocking loadings are presented to demonstrate the effectiveness and efficiency of the proposed scheme .The numerical results will be presented in the nondimensional forms. In the numerical investigations, spatial dilution of vibrations and attenuation due to material damping of half-space medium will be discussed. Also, some comments about the presented scheme and numerical results will be made.

Analytical Model for Half-space Medium

The analytical model is a rigid circular plate on a half-space medium subjected to time harmonic loadings. The interaction tractions between plate and surrounding medium are shown in Fig.1, and can be expressed in cylindrical coordinates in terms of Fourier components with respect to azimuth.

$$\begin{bmatrix} \overline{\tau_{rz}}(r,\theta) \\ \overline{\sigma_{zz}}(r,\theta) \\ \overline{\tau_{\theta z}}(r,\theta) \end{bmatrix} e^{i\omega t} = \sum_{n=0}^{1} \begin{bmatrix} \overline{\tau_{rz}}^{n}(r) \begin{Bmatrix} \cos(n\theta) \\ \sin(n\theta) \end{Bmatrix} \\ \overline{\sigma_{zz}}^{n}(r) \begin{Bmatrix} \cos(n\theta) \\ \sin(n\theta) \end{Bmatrix} \\ \overline{\tau_{\theta z}}^{n}(r) \begin{Bmatrix} -\sin(n\theta) \\ \cos(n\theta) \end{Bmatrix} \end{bmatrix} e^{i\omega t} \quad ; \quad 0 \le r \le a_0 \tag{1}$$

where the superscript n denotes the n^{th} Fourier component in the series; in this circular plate case, $n = 0$ represents vertical (symmetric with respect to θ=0) and torsional loadings (anti-symmetric), $n = 1$ represents horizontal and rocking loadings (symmetric); ω = frequency; and a_0 is radius of circular plate. Since the time variation $e^{i\omega t}$ appears on both sides of the equation and can therefore be canceled, it is omitted hereinafter.

To solve 3D wave equations with prescribed tractions given by Eq(1), some fundamental solutions can be exploited. Sezawa [14] developed a technique for separating the dilatational and rotational waves in the general equations of wave propagation, and used the technique of separation of variables to obtain general solution for n^{th} Fourier component with respect to azimuth. After mathematical manipulations of the general solution, one can express the displacement components at the surface z=0 in terms of the traction components on the surface for any n^{th} Fourier component as follows:

$$\begin{bmatrix} u_r(r,0) \\ u_z(r,0) \\ u_\theta(r,0) \end{bmatrix} = \mathbf{J} \begin{bmatrix} -\nu' k_\beta^2/\Lambda & k(2\nu\nu' - 2k^2 + k_\beta^2)/\Lambda & 0 \\ k(2\nu\nu' - 2k^2 + k_\beta^2)/\Lambda & -\nu k_\beta^2/\Lambda & 0 \\ 0 & 0 & -1/G\nu' \end{bmatrix}$$

$$\boldsymbol{J}^{-1}\begin{bmatrix}\tau_{rz}(r,0)\\ \sigma_{zz}(r,0)\\ \tau_{\theta z}(r,0)\end{bmatrix} \tag{2a}$$

or

$$\boldsymbol{u}_0 = \boldsymbol{J}\,\boldsymbol{Q}\,\boldsymbol{J}^{-1}\boldsymbol{t}_0 \tag{2b}$$

where

$$\boldsymbol{J}=\begin{bmatrix}J_n'(kr) & 0 & (n/r)J_n(kr)\\ 0 & kJ_n(kr) & 0\\ (n/r)J_n(kr) & 0 & J_n'(kr)\end{bmatrix} \tag{2c}$$

$\Lambda = G[4k^2 v v' - (2k^2 - k_\beta^2)^2]$; $v = \sqrt{k^2 - (\omega^2/c_p^2)}$; $v' = \sqrt{k^2 - (\omega^2/c_s^2)}$

; $k_\beta = \dfrac{\omega}{c_s}$; c_P and c_s = compressional and shear wave velocities; G = shear modulus; k = wave number in the horizontal direction; $J_n'(kr)$ = first kind of Bessel function of order n; and $J_n'(kr) = [dJ_n(kr)/dr]$.

In order to simulate the arbitrary distributions of interaction tractions in r-direction , the distribution of tractions in r-direction of Eq.(1) is approximated by piecewise linear model with respect to r-direction of cylindrical coordinates. Assuming that the interval $(0, a_0)$ for Eq. (1) is divided into m subintervals with equal width $b = \dfrac{a_0}{m}$, one can express the piecewise linear stress distribution as follows:

$$\begin{aligned}\overline{\tau_{rz}} &= \sum_{j=1}^{m-1} h_j(r)p_j + h_0(r)p_0 + h_m(r)p_m = \boldsymbol{h}^T\boldsymbol{p}\\ \overline{\sigma_{zz}} &= \sum_{j=1}^{m-1} h_j(r)q_j + h_0(r)q_0 + h_m(r)q_m = \boldsymbol{h}^T\boldsymbol{q}\\ \overline{\tau_{\theta z}} &= \sum_{j=1}^{m-1} h_j(r)s_j + h_0(r)s_0 + h_m(r)s_m = \boldsymbol{h}^T\boldsymbol{s}\end{aligned} \tag{3}$$

where

$$h_j(r)=\begin{cases} 1+\dfrac{r-jb}{b}, & \textbf{if} \quad (j-1)b\le z\le jb \quad and \quad 1\le j\le m \\ 1-\dfrac{r-jb}{b}, & \textbf{if} \quad jb\le z\le (j+1)b \quad and \quad 0\le j\le m-1 \\ 0, & otherwise, \end{cases} \tag{3a}$$

and p_j, q_j and s_j are the traction intensities at node j for $\overline{\tau_{rz}}$, $\overline{\sigma_{zz}}$ and $\overline{\tau_{\theta z}}$ respectively. Liou [11] has developed a technique to decompose the tractions in Eq.(3) as follows:

$$\begin{aligned}
\begin{bmatrix} \overline{\tau_{rz}}(r) \\ \overline{\sigma_{zz}}(r) \\ \overline{\tau_{\theta z}}(r) \end{bmatrix} &= \begin{bmatrix} 1 \\ 0 \\ -1 \end{bmatrix}\left(\frac{\overline{\tau_{rz}}(r)-\overline{\tau_{\theta z}}(r)}{2}\right)+\begin{bmatrix} 0 \\ 1 \\ 0 \end{bmatrix}\overline{\sigma_{zz}}(r)+\begin{bmatrix} 1 \\ 0 \\ 1 \end{bmatrix}\left(\frac{\overline{\tau_{rz}}(r)+\overline{\tau_{\theta z}}(r)}{2}\right) \\
&= \begin{bmatrix} 1 \\ 0 \\ -1 \end{bmatrix}\frac{1}{2}\left[\mathbf{h}^T,\mathbf{0},\mathbf{h}^T\right]\begin{bmatrix} \mathbf{p} \\ 0 \\ \mathbf{s} \end{bmatrix}dk \\
&+\begin{bmatrix} 0 \\ 1 \\ 0 \end{bmatrix}\left[\mathbf{0},\mathbf{h}^T,\mathbf{0}\right]\begin{bmatrix} 0 \\ \mathbf{q} \\ 0 \end{bmatrix}dk \\
&+\begin{bmatrix} 1 \\ 0 \\ 1 \end{bmatrix}\frac{1}{2}\left[\mathbf{h}^T,\mathbf{0},\mathbf{h}^T\right]\begin{bmatrix} \mathbf{p} \\ 0 \\ \mathbf{s} \end{bmatrix}dk \\
&= \int_0^\infty \begin{bmatrix} 1 \\ 0 \\ -1 \end{bmatrix} kJ_{n+1}(kr)\left[\mathbf{D}_{n+1}{}^T,\mathbf{0},\mathbf{D}_{n+1}{}^T\right]\begin{bmatrix} \mathbf{p} \\ 0 \\ \mathbf{s} \end{bmatrix}dk \\
&+\int_0^\infty \begin{bmatrix} 0 \\ 1 \\ 0 \end{bmatrix} kJ_n(kr)\left[\mathbf{0},\mathbf{D}_n,\mathbf{0}\right]\begin{bmatrix} 0 \\ \mathbf{q} \\ 0 \end{bmatrix}dk \\
&+\int_0^\infty \begin{bmatrix} 1 \\ 0 \\ 1 \end{bmatrix} kJ_{n-1}(kr)\left[\mathbf{D}_{n+1},\mathbf{0},\mathbf{D}_{n+1}\right]\begin{bmatrix} \mathbf{p} \\ 0 \\ \mathbf{s} \end{bmatrix}dk
\end{aligned} \tag{4}$$

where

$$\boldsymbol{D}_{n+1}^{T} = \int_0^{a_0} \frac{r}{2} J_{n+1}(kr)\boldsymbol{h}^{\boldsymbol{T}} dr$$

$$\boldsymbol{D}_{n}^{T} = \int_0^{a_0} r J_{n+1}(kr)\boldsymbol{h}^{\boldsymbol{T}} dr \tag{4a}$$

and

$$\boldsymbol{D}_{n-1}^{T} = \int_0^{a_0} \frac{r}{2} J_{n-1}(kr)\boldsymbol{h}^{\boldsymbol{T}} dr$$

The integrals on the right hand side of Eq.(4) and integrals in Eqs.(4a) are Hankel transform pairs respectively. One should also notice that the vectors $(1,0,-1)^T$, $(0,1,0)^T$ and $(1,0,1)^T$ are orthogonal eigenvectors corresponding to eigenvalue $-kJ_{n+1}(kr)$, $kJ_n(kr)$ and $kJ_{n-1}(kr)$ of the Bessel functions matrix $\boldsymbol{J}$ in Eq.(2c). Therefore, Eq.(4) can be replaced with the following equation.

$$\begin{bmatrix} \overline{\tau_{rz}} \\ \overline{\sigma_{zz}} \\ \overline{\tau_{\theta z}} \end{bmatrix} = \int_0^{\infty} \boldsymbol{J} \begin{bmatrix} -\boldsymbol{D}_{n+1}^{T} + \boldsymbol{D}_{n-1}^{T} & 0 & \boldsymbol{D}_{n+1}^{T} + \boldsymbol{D}_{n-1}^{T} \\ 0 & \boldsymbol{D}_{n}^{T} & 0 \\ \boldsymbol{D}_{n+1}^{T} + \boldsymbol{D}_{n-1}^{T} & 0 & -\boldsymbol{D}_{n+1}^{T} + \boldsymbol{D}_{n-1}^{T} \end{bmatrix} \begin{Bmatrix} \boldsymbol{q} \\ \boldsymbol{p} \\ \boldsymbol{s} \end{Bmatrix} dk \tag{5}$$

$$= \int_0^{\infty} \boldsymbol{JDP} \quad dk$$

Using $\boldsymbol{t_0} = \boldsymbol{-\overline{t_0}}$ and substituting $\boldsymbol{t_0} = \boldsymbol{-JDP} \quad dk$ from Eq. (5) into Eq. (2b), the following equation can be obtained by integrating the resulting expression from 0 to ∞.

$$\boldsymbol{u_0} = -\int_0^{\infty} \boldsymbol{JQDP} \quad dk \tag{6}$$

Eq.(6) defines the relationship between displacement vector and prescribed traction on the surface for the n^{th} Fourier component. To generate the impedance matrix, substructuring concept, principle of virtual work and reciprocal theorem will be used.

Consider half-space medium with the prescribed tractions defined by Eq. (3) which approximates Eq.(1) for tractions. Variational principle gives

$$\begin{aligned}\delta W &= \int_0^{a_0}\int_0^{2\pi} \delta \overline{\boldsymbol{t}_0}^{\boldsymbol{T}} \boldsymbol{u_0} r d\theta dr \\ &= -\begin{pmatrix} 2\pi \\ \pi \end{pmatrix} \delta \boldsymbol{P}^T \int_0^{a_0} \boldsymbol{H} \int_0^{\infty} \boldsymbol{JQD} dk r dr \boldsymbol{P} \\ &= -\begin{pmatrix} 2\pi \\ \pi \end{pmatrix} \delta \boldsymbol{P}^T \int_0^{\infty} \left(\int_0^{a_0} \boldsymbol{HJ} r dr \right) \boldsymbol{QD} dk \boldsymbol{P}\end{aligned} \tag{7}$$

where matrix $\boldsymbol{H} = diag(\boldsymbol{h},\boldsymbol{h},\boldsymbol{h})$, and $\boldsymbol{h}$, $\bar{\boldsymbol{t}}_0$ and $\boldsymbol{u_0}$ are defined in Eqs. (3) and (6) . The coefficients 2π and π in Eqs. (7) come from the integrals $\int_0^{2\pi} \cos^2 n\theta d\theta$ or $\int_0^{2\pi} \sin^2 n\theta d\theta$ which are not explicitly expressed in the formulations. Furthermore, using the procedure developed to obtain Eq. (4), one can show that

$$\int_0^{a_0} \boldsymbol{HJ} r dr = k\boldsymbol{D}^T \tag{8}$$

where the matrix $\boldsymbol{D}$ is defined in Eqs. (5) and (4a). The virtual work in Eq.(7) can then be rewriteen in the form as follows:

$$\begin{aligned}\delta W &= -\begin{pmatrix} 2\pi \\ \pi \end{pmatrix} \delta \boldsymbol{P}^T \int_0^{\infty} \boldsymbol{D}^{\boldsymbol{T}} \boldsymbol{QD} dk dk \boldsymbol{P} \\ &= \begin{pmatrix} 2\pi \\ \pi \end{pmatrix} \delta \boldsymbol{P}^T \boldsymbol{K} \boldsymbol{P}\end{aligned} \tag{9}$$

Using Eq.(2a) or Bettis's Theorem, one can show that the matrix $\boldsymbol{Q}$ is symmetric. Therefore, matrix $\boldsymbol{K} = -\int_0^{\infty} \boldsymbol{D}^{\boldsymbol{T}} \boldsymbol{QD} dk dk$ is also symmetric.

Now, consider the plate itself. Similar to finite element modeling, the displacement field of the plate for n^{th} Fourier component can be assumed as:

$$\bar{\boldsymbol{u}}_0 = \boldsymbol{N}\boldsymbol{v}\begin{pmatrix}\cos n\theta \\ \sin n\theta\end{pmatrix} \tag{10}$$

where matrix $\boldsymbol{N}$ is comprised of the shape functions in r-direction, and vector $\boldsymbol{v}$ is comprised of the generalized displacements at the nodal rings of the plate finite element model. Similarly, variational principle gives:

$$\begin{aligned}\delta W &= \int_0^{2\pi}\int_0^{a_0} \delta\bar{\boldsymbol{t}}_0^{\boldsymbol{T}}\bar{\boldsymbol{u}}_0 r dr d\theta \\ &= \begin{pmatrix}2\pi \\ \pi\end{pmatrix}\delta\boldsymbol{P}^T\int_0^{a_0}\boldsymbol{H}\boldsymbol{N}r dr\boldsymbol{v} \\ &= \begin{pmatrix}2\pi \\ \pi\end{pmatrix}\delta\boldsymbol{P}^T\boldsymbol{B}\boldsymbol{v}\end{aligned} \tag{11}$$

Equating Eq. (11) to Eq. (9) and factoring out $\delta\boldsymbol{P}^T$, it is obtained

$$\begin{pmatrix}2\pi \\ \pi\end{pmatrix}\boldsymbol{K}\boldsymbol{P} = \begin{pmatrix}2\pi \\ \pi\end{pmatrix}\boldsymbol{B}\boldsymbol{v} \tag{12}$$

$$\boldsymbol{P} = \boldsymbol{K}^{-1}\boldsymbol{B}\boldsymbol{v} \tag{13}$$

or

$$\boldsymbol{V} = \begin{pmatrix}2\pi \\ \pi\end{pmatrix}\boldsymbol{B}v \tag{14}$$

where vector $\boldsymbol{V}$ are the generalized displacements at the nodal rings of the assumed piecewise linear stress model. Eq. (14) gives the relationship between the nodal generalized displacements of the assumed stress model of Eqs.(3) and the displacements of the finite element model of Eq. (10). To obtain the corresponding force-traction relationship for both models, reciprocal theorem can be used. This leads to the following equation.

$$\boldsymbol{F} = \begin{pmatrix}2\pi \\ \pi\end{pmatrix}\boldsymbol{B}^T\boldsymbol{P} \tag{15}$$

where vector $\boldsymbol{F}$ are the generalized forces at the nodal rings of the finite element model. Substituting Eq. (13) into Eq. (15) yields

$$\boldsymbol{F} = \begin{pmatrix} 2\pi \\ \pi \end{pmatrix} \boldsymbol{B}^T \boldsymbol{K}^{-1} \boldsymbol{B} \boldsymbol{v} = \boldsymbol{I} \boldsymbol{v} \tag{16}$$

The matrix $\boldsymbol{I}$ is the impedance matrix for n^{th} Fourier component.

Eq.(16) gives the relationship of applied force and plate vibration displacement. For finding vibration at any specific location on half-space medium, Eq.(16) will be employed to calculate plate vibration $\boldsymbol{v}$ induced by the external applying harmonic force $\boldsymbol{F}$ first, the vector $\boldsymbol{P}$ of traction intensities at nodal rings is calculated by Eq.(13) secondly, and then Eq.(6) is used to calculate the vibration at any specific location. Although Eq.(6) does not show the variation of vibration with respect to azimuth θ, the variation with respect to θ can be obtained by simply multiplying $\cos\theta$ or $\sin\theta$ for rocking and horizontal loadings as shown in Eq.(1). Numerical results of plate impedance functions have been shown by Liou et al [13]. Therefore, the main purposed of the paper is to employ Eq.(6) to calculate the vibration at any specific location on a half-space medium.

Numerical Investigation

In the semi-infinite integrations of Eq. (6) and (9), singular point may exist, provided there is no damping assumed for half-space medium. This is because $\Lambda = 0$ in matrix $\boldsymbol{Q}$ in Eq.(2a) when wave number k is equal to Rayleigh wave number. Although technique such as residue theorem may be used to calculate the integration around the singular point, material damping is introduced in half-space medium in order to comply with the more realistic situation of medium, and hysteretic type of damping is chosen. This means shear modulus G in Eqs.(2) is complex and can be expressed as $G = \overline{G}(1 + 2\xi i)$ in which ξ is damping ratio. Therefore, numerical integration scheme can be directly employed. In the study, Poisson ratio of half-space medium is assumed to be 0.33. Furthermore, using the following two statements, the integrand in the semi-infinite integral of Eq.(9) can be easily shown to be proportional to $\frac{1}{k^3}$ and the integrand in Eq.(6) is proportional to $\frac{1}{k^2}$ as $k \to \infty$:

(1) The elements of matrix $\boldsymbol{Q}$ decay with $\frac{1}{k}$ as $k \to \infty$, since $\nu \doteq \nu' \doteq k$ as $k \to \infty$.

(2) Using the identities of $\int r^2 J_n(kr)dr = -\frac{r^2}{k} J_{n+1}(kr) + \frac{n+1}{k} \int r J_{n-1}(kr)dr$ and $\int r J_n(kr)dr = -\frac{r}{k} J_{n-1}(kr) + \frac{n}{k} \int J_{n-1}(kr)dr$, and $J_n(kr) \propto \frac{1}{k^{0.5}}$ as $k \to \infty$, it is concluded that the elements of matrix $\boldsymbol{D}$ in Eqs.(4), (4a), (5), (6) and (9) decay with $\frac{1}{k^{1.5}}$. It is therefore appropriate to replace the infinite integration limit with a finite number without losing accuracy.

After some convergence study, the followings can be concluded : (1) $m = 20$ for the number of subinterval in Eqs.(3) is enough to accurately describe the distribution of interaction tractions between plate and half-space medium; (2) To approximate the semi-infinite integrals of Eqs.(6) and (9), the upper limit of integration is controlled by Eq.(6), Since the integrand in Eq.(9) is proportional to $\frac{1}{k^3}$ and integrand in Eq.(6) is

proportional to $\frac{1}{k^2}$ as $k \to \infty$; (3) In general, the upper limit of integration in Eq.(6) must be larger as the nondimensional distance from plate center is further, hysteretic damping ratio of half-space medium is greater, or excitation frequency is higher.

The above mentioned third conclusion except first part is related to the phenomenon of Rayleigh wave behavior. Let us look at Bessel function matrix J in Eqs.(6) and (2c). The elements in matrix J is proportional to $k^{0.5}$ as $k \to \infty$. And the elements in matrix $\boldsymbol{Q}$ and $\boldsymbol{D}$ in Eq.(6) are independent of R (the distance from vibration source). This means larger R needs larger upper limit of integration in Eq.(6) to compensate the integration accuracy. This leads to the first part of third conclusion. Also, high damping will make $\frac{1}{\Lambda}$ in Q matrix smaller for k in the neighborhood of Rayleigh wave number. This means Rayleigh wave number component is less dominating the value of the integration in Eq.(6). This explains the second part of third conclusion. For the case of higher excitation frequency, the upper limit of integration in Eq.(6) must be larger due to higher respective Rayleigh wave number. This statement reasons the third part of third conclusion.

To obtain certain accuracy, it is difficult to definitely give a clear rule to set the upper integration limit in Eq.(6), since the above three stated factors influence the upper integration limit in different proportions. Therefore, one can only employ the above third conclusion as a guide line and increase the upper integration limit to check if the results of vibrations calculated by Eq.(6) is converging.

Since the total system is linear. All the quantities can be nondimensionalized. As shown in Reference 13, the torsional, vertical, horizontal, coupling and rocking impedance functions are nondimensionalized respectively as follow: $\frac{I_{TT}}{Ga_0^3}$, $\frac{I_{vv}}{Ga_0}$, $\frac{I_{HH}}{Ga_0}$, $\frac{I_{HR}}{Ga_0^2}$, and $\frac{I_{RR}}{Ga_0^3}$. Therefore, the excitation forces are normalized in the similar way. However, in order to obtain nondimensional displacements u_r, u_z and u_θ in Eq.(6), the shear wave length for $1\ Hz$ $(\frac{\omega}{2\pi} = 1)$ frequency is introduced. The wave length $\lambda = Re(c_s)/1\ \sec.$, in which $Re(c_s)$ is real part of shear wave velocity c_s. Complex

c_s is due to complex shear modulus G. The vertical and horizontal excitation forces are nondimensionalized in the forms of $\frac{F_V}{Ga_0\lambda}$ and $\frac{F_H}{Ga_0\lambda}$ respectively. The torsional and rocking excitation moments are normalized in the forms of $\frac{M_T}{Ga_0^3\lambda}$ and $\frac{M_R}{Ga_0^3\lambda}$ respectively. The reason to manipulate the quantities in this way is to made the following numerical results of u_r, u_z and u_θ have been nondimensionalized by λ. The numerical results shown in the following figures are produced by unit harmonic excitation forces. This means $\frac{F_V}{Ga_0\lambda}$, $\frac{F_H}{Ga_0\lambda}$, $\frac{M_T}{Ga_0^3\lambda}$ or $\frac{M_R}{Ga_0^3\lambda} = 1$.

In the numerical results, the hysteretic damping ratios $\xi = 0.0001,\ 0.001,\ 0.01,\ 0.02,\ 0.03$ and 0.05 are selected for half-space medium. The reason to select the case of very low damping ($\xi = 0.0001$) is to check and approximate the behavior of vibration in the medium without material damping. Figs. 2-13 show the results of vibration amplitudes along the nondimensional distance from center of circular plate. In Figs. 2-13, the distance R is nondimensionalized as $\frac{\omega R}{2\pi Re(c_s)}$ in which ω is excitation frequency. Figs. 2-13 show the results for the case of nondimensional frequency $\frac{\omega a_0}{2\pi Re(c_s)} = 0.00005$. This small nondimensional frequency can be used to approximate point source exaitation problem. Fig. 2 shows the vibration amplitude of u_θ component due to unit normalized torsional moment excitation. From the figure, one can see that for $\frac{\omega R}{2\pi Re(c_s)} \le 0.5$ the attenuation of vibration in mainly caused by spatial dilution and for $\frac{\omega R}{2\pi Re(c_s)} \ge 0.5$ material damping is getting more significant for attenuation of vibration. Also, the vibration decays along the distance smoothly. Figs.3 and 4 show the vibration amplitudes of u_r and u_z respectively due to unit nondimensional vertical force. Looking at these two figures, one can observe that the vibration attenuate over the distance only from marco view of point, the amplitudes of vibration along the distance fluctuate, the fluctuation becomes more dramatic as damping getting higher and the period of the

fluctuation over the nondimensional distance is around 1.90. To explain these phenomena, one can refer to Eqs.(6) and (2a). The $\frac{1}{\Lambda}$ in Q matrix of Eqs.(6) or (2a) will be getting huge as k is close to Rayleigh wave number. Rayleigh wave number is approximately $1.073\frac{\omega}{Re(c_s)}$ for poisson ratios 0.33 . Therefore, the contribution of the wave number components in the neighborhood of Rayliegh wave number is very important in the integration of Eq.(6). Dependent upon distance, this property will make the value of the integration of Eq.(6) larger or smaller locally. The fluctuation is caused by this property. Furthermore, the Rayleigh wave length is about $0.932\frac{2\pi Re(c_s)}{\omega}$. This is about half of the period of fluctuation along nondimensional distance in Figs.3 and 4. One should also notice that the phenomenon mentioned above does not occur in the torsional case (Fig.2). For torsional excitation, only SH wave is generated.

The above mentioned interesting phenomenon leads to the curiosity of finding the average energy flux intensity at $z=0$. The average flux intensity can be easily calculated by the formula as follows:

$$\overline{E}=\rho\omega^2\frac{\omega}{2\pi}\frac{1}{2\pi}\int_0^{\frac{\omega}{2\pi}}\int_0^{2\pi}(|u_r|^2+|u_z|^2+|u_\theta|^2)\begin{pmatrix}sin^2n\theta\\cos^2n\theta\end{pmatrix}d\theta\quad e^{2i\omega t}dt \tag{17}$$

Where ρ is mass density. The flux intensity in Eq.(17) is averaging over time period $\frac{2\pi}{\omega}$ and circle length $2\pi R$. Eq.(17) is easy to be integrated. The $\overline{E}$ can be normalized to become the following equation without lossing the meaning of average energy flux intensity.

$$E=|u_r|^2+|u_z|^2+|u_\theta|^2 \tag{18}$$

Now, one can employ Eq.(18) to calculate E for different distances from the center of plate. The results are shown in Fig.5. From the figure, one observes that the fluctuation is smaller. It is also believed that the curve for average energy flux intensity will be smoother

for greater z , since Rayleigh wave is confined in the depth near free surface.

Figs. 6~8 show the results of three components u_r, u_z and u_θ induced by unit nondimensional horizontal excitation. Comparing these three figures to Figs. 4-5, one can observe similar phenomenon of local fluctuation except the fluctuation becomes more dramatic. Eq.(18) is employed to calculate the average energy flux intensity at $z = 0$ induced by unit nondimensional horizontal excitation. The results are shown in Fig.9. From the figure, one can see that the fluctuation is greatly reduced. For the case of unit normalized rocking excitation, Figs. 10-12 show the results of the three components u_r, u_z and u_θ. From these three figures, similar fluctuation phenomenon is observed. However, the fluctuation is less dramatic. Also, Eq.(18) is used to compute the average energy flux intensity and the results are shown in Fig.13. Again, the fluctuation for the results of average energy flux intensity is dramatically reduced.

Concluding Remarks

After extensive numerical investigations of the presented scheme, the following conclusions and suggestions can be made.

(1) For nondimensional distance $(\frac{\omega R}{2\pi Re(c_s)})$ is smaller than 0.5, the decay of vibration is mainly governed by spatial dilution of waves. For $(\frac{\omega R}{2\pi Re(c_s)}) > 2.0$, the decay of vibration is mainly governed by material damping of half-space medium. For $0.5 \le (\frac{\omega R}{2\pi Re(c_s)}) \le 2.0$, both spatial dilution and material damping have the influence on vibration attenuation.

(2) One should not jump to conclusion that the vibration components $(u_r,\ u_z\ \ and\ \ u_\theta)$ are smaller as the distance from vibration source is further. From macro view, the vibration does attenuate over the distance from vibration source. However, there are fluctuations of vibration amplitudes along distance as shown in some above mentioned figures.

(3) Although the results of vibrations for the cases of high nondimensional frequencies are not shown in the paper, the fluctuation for the cases of high frequencies is even more severe, and the period of fluctuation along nondimensional distance is always about twice of Rayleigh wave length.

(4) The presented procedure can be extended to deal with the cases of layered half-space medium, calculating vibrations at locations with depth $z \neq 0$ and plates with arbitrary shapes. For the cases of layered half-space medium and calculating vibration at depth $z \neq 0$, one just need to revise Q matrix in Eqs.(2a) and (6). For the case of plates with arbitrary shapes, one just need to incorporate more Fourier components as indicated in Eq.(1) in the calculation.

(5) According Eq.(10), the presented procedure is feasibly combined with finite element model of superstructure on foundation plate. This would take soil-structure interaction effect into account.

References

[1] Colin G. Gordon, Thomas L. Dresner, “Methods of developing virbration and acoustic noise specifications for microelectronics process tools” Vibration Monitoring and Control SPIE Proceedings Volume 2264, July 1994.

[2] X. Sheng, C. J. C. Jones, M. Petyt, “Ground vibration generated by a load moving along a railway track ”, Journal of Sound and Vibration, 228(1) (1999), 129-156.

[3] V. V. Krylov, “Vibrational impact of high-speed trains. I. Effect of track dynamics. ”, Journal of the Acoustical Society of America, 100(5) (1996), 3121-3134.

[4] Amir M. Kaynic, Christian Madshus, Peter Zackrisson, “Ground vibration from high-speed train: prediction and countermeasure.”Journal of Geotechnical and Geoenvironmental Engineering , 126 (6) (2000), 0531-0573.

[5] Hirokazu Takemiya, Xuecheng Bian, “Substructure simsulation of inhomogeneous track and layered ground dynamic interaction under train passage” Journal of Engineering Mechanics, 131(7) (2005), 699-711.

[6] Hirokazu Takemiya, “Simulation of track-ground vibrations due to high-speed train: the case of X-2000 at Ledsgard ” Journal of Sound Vibration, (261)(2003), 503-526.

[7] S. Ahmad, TM. A1-Hussaini, “Simplified design for vibration screening by open and in-filled trenches.” J Geotech Engineering, ASCE 117(1) (1991), 67-88.

[8] B. Dasgupta, DE. Beskos, and IG. Vardoulakis, “Vibration isolation using open or filled trenches part 2 3D homogenous soil” Comput Mech (1990),129-42.

[9] Hirokazu Takemiya, “Field vibration mitigation by honeycomb WIB for pile foundations of a high-speed train viaduct” Soil Dynamics and Earthquake Engineering, (24)(2004),69-87.

[10] G. F. Miller, H. Pursey. “On the partition of energy between elastic waves in a semi-infinite solid” The Royal Society of London. Series A, Mathematical and Physical Sciences, 233 (6) (1955), 55-69.

[11] R. D. Woods, P. J. Larry, “Energy-Attenuation Relationships from Construction Vibrations,” Proceedings of Vibration Problems in Geotechnical Engineering Convention, Detroit, Michigan(1985), 229-246.

[12] G.-S. Liou, “Analytical solution for soil-structure interaction in layered media.” J. of Earthquake Engineering. And Struct. Dynamics, 18(5) (1989), 667-686.

[13] Gin-Show Lion, George C. Lee. “Analytic solution for dynamic loading on half-space medium.” Journal of Engineering Mechanics, 117(7)(1991), 0007-1485.

[14] K. Sezawa, “Further studies on Rayleigh waves having some azimuthal distribution.” Bulletin of Earthquake Res. Inst., Tokyo, Japan, 6(1)(1929), 1-81.

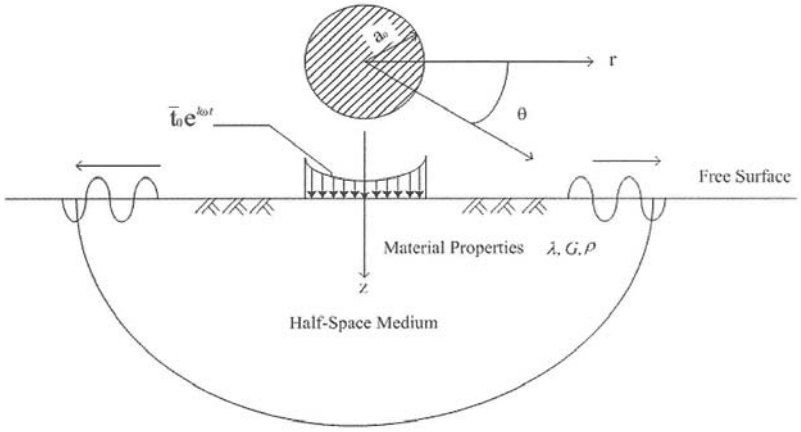

Fig. 1: Dynamic Loading on Half-Space Medium

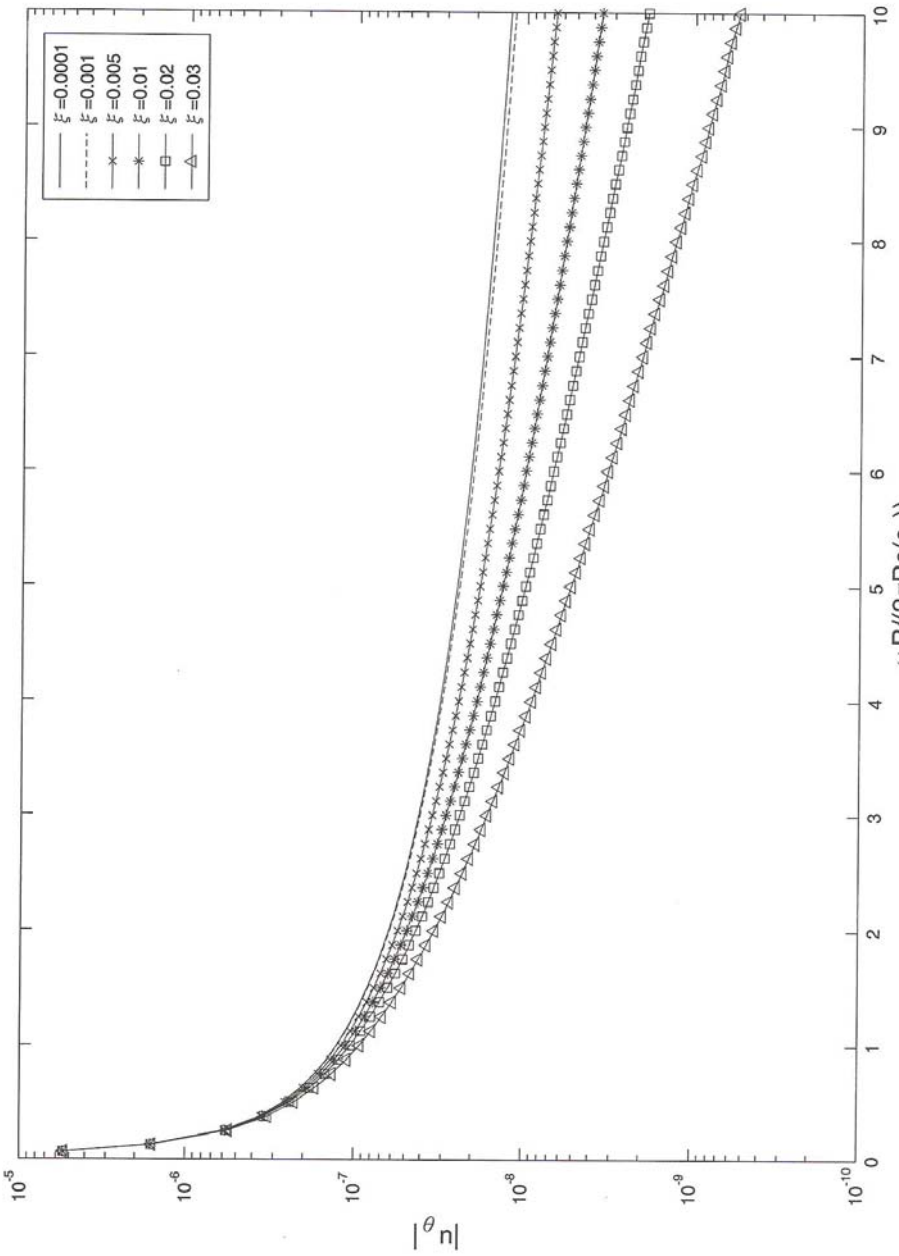

Fig.2: Vibration Amplitude of u_θ due to Unit Normalized Torsional Excitation

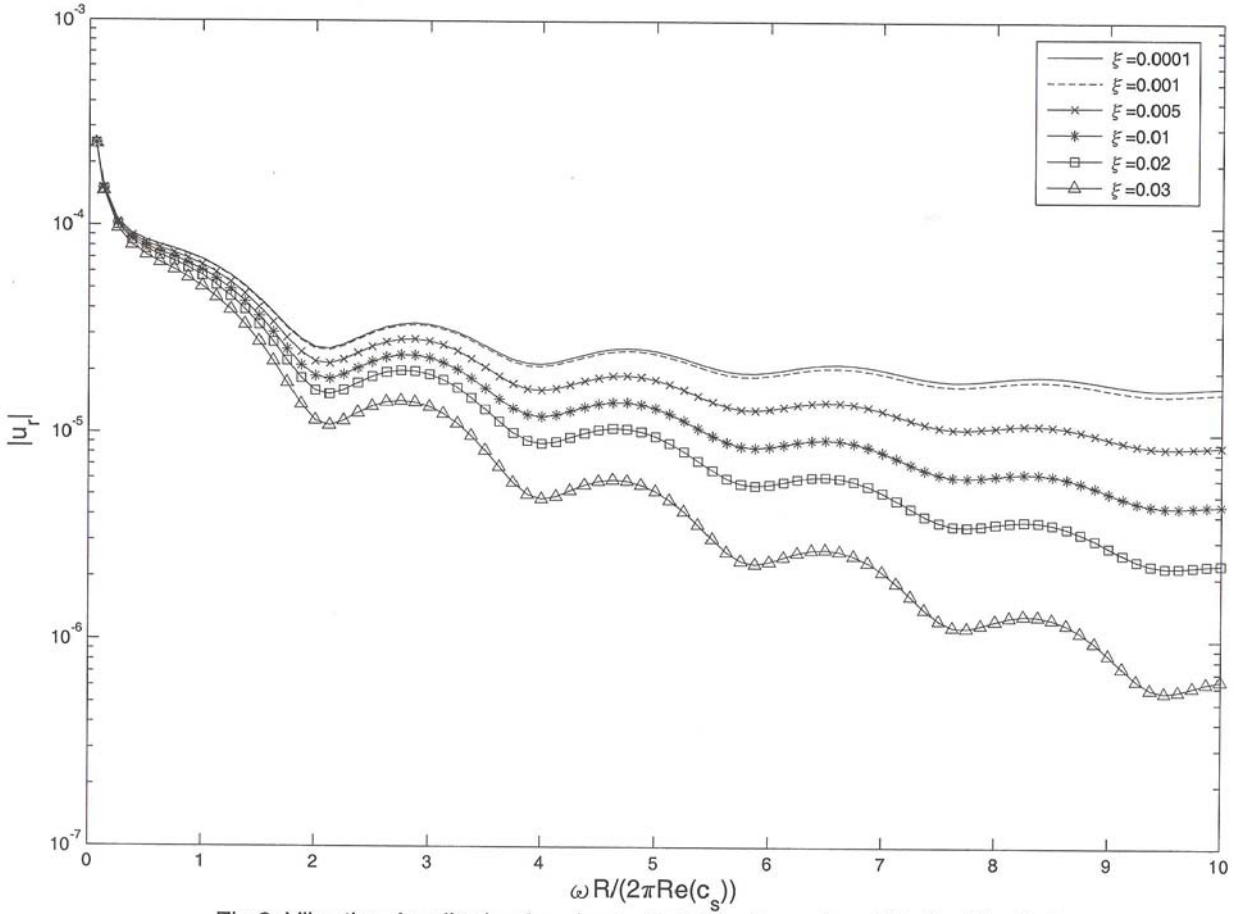

Fig.3: Vibration Amplitude of u_r due to Unit Nondimensional Vertical Excitation

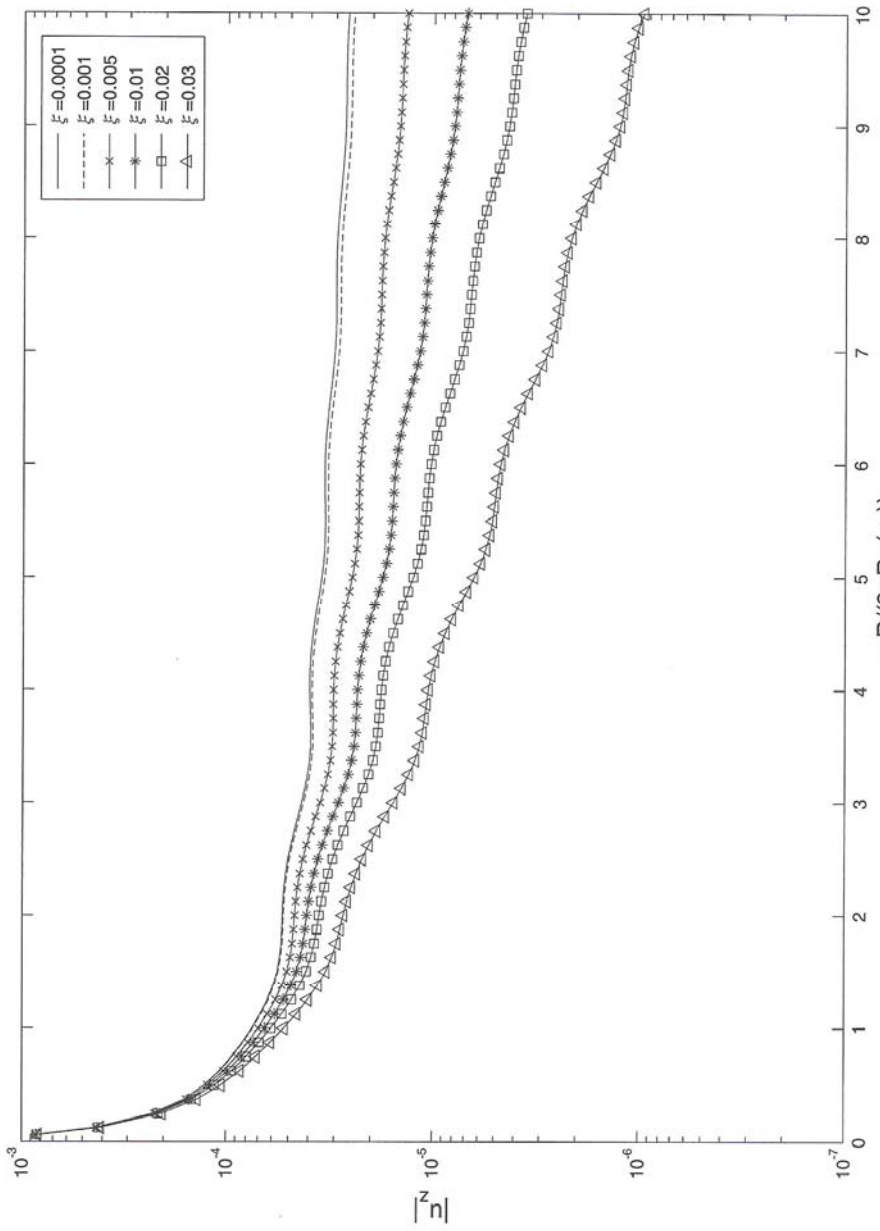

Fig.4: Vibration Amplitude of u_z due to Unit Nondimensional Vertical Excitation

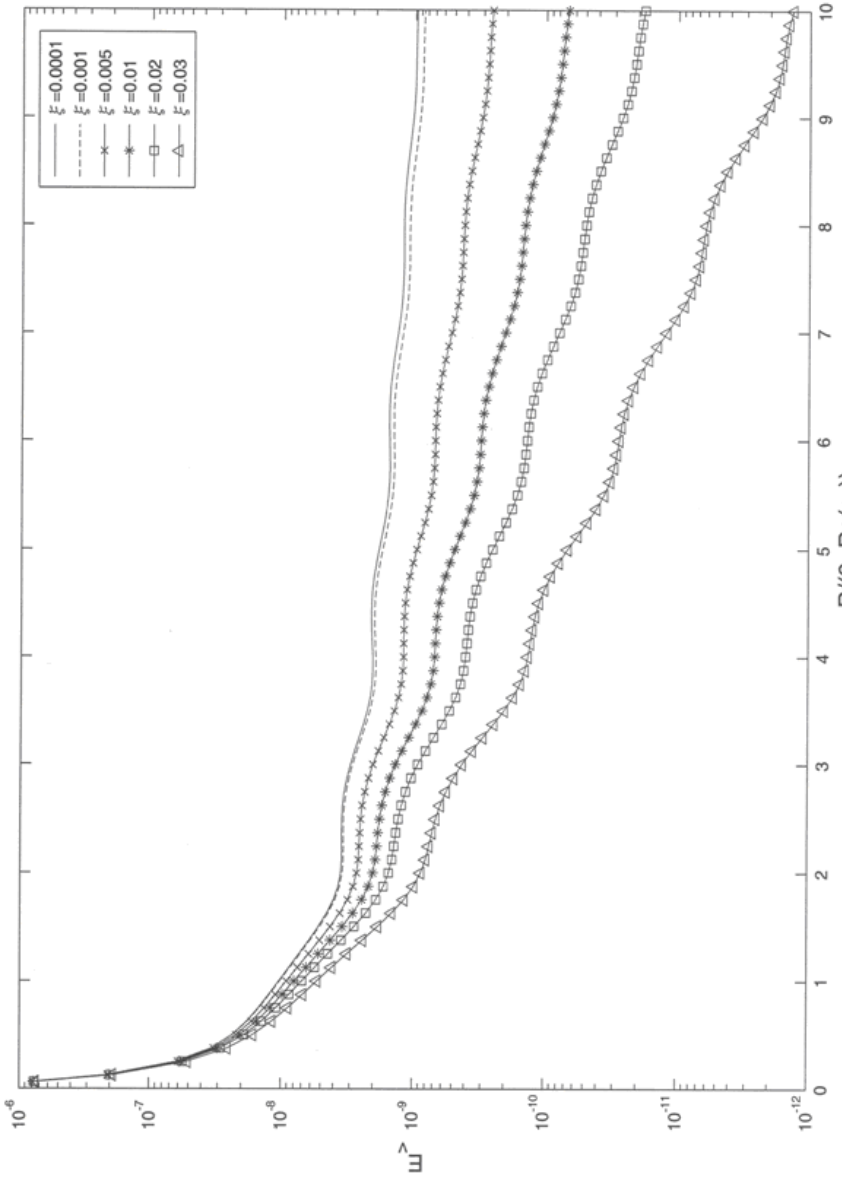

Fig.5: Average Energy Flux Intensity due to Unit Nondimensional Vertical Excitation

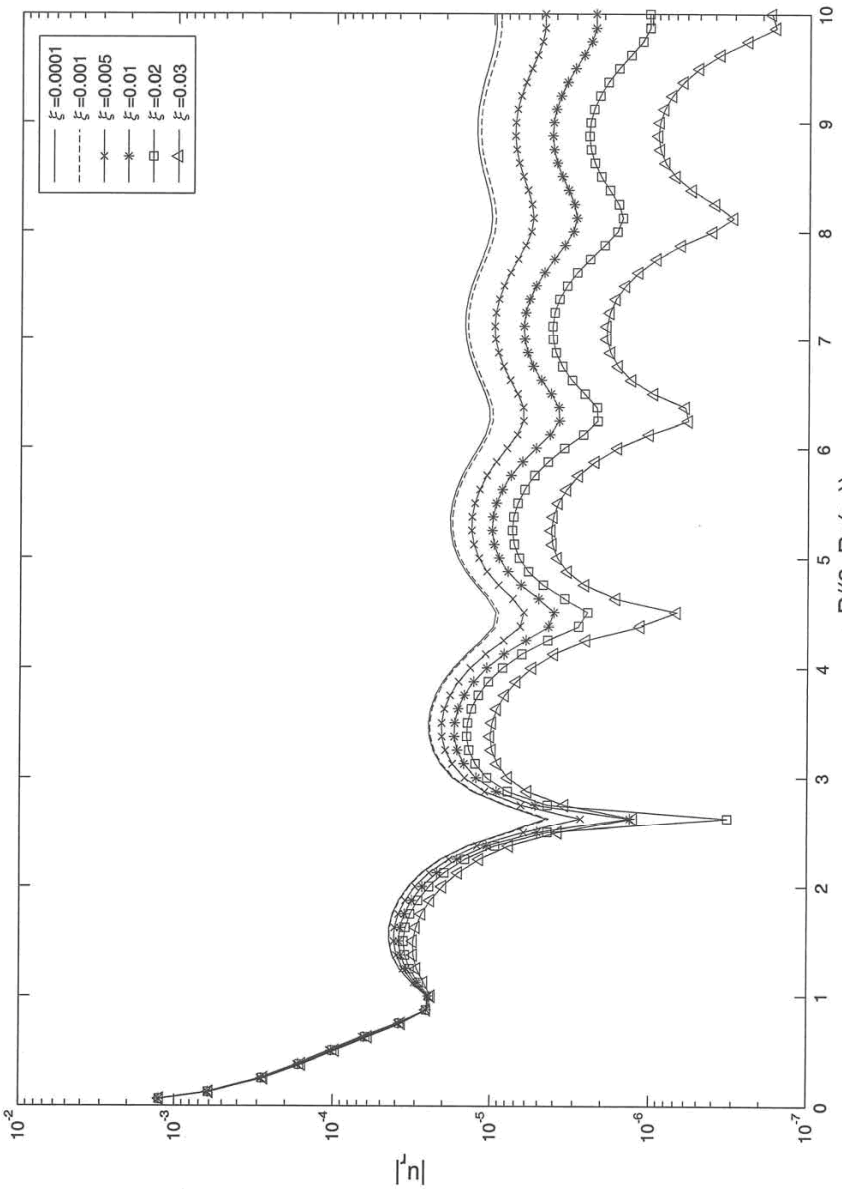

Fig.6: Vibration Amplitude of u_r due to Unit Nondimensional Horizontal Excitation

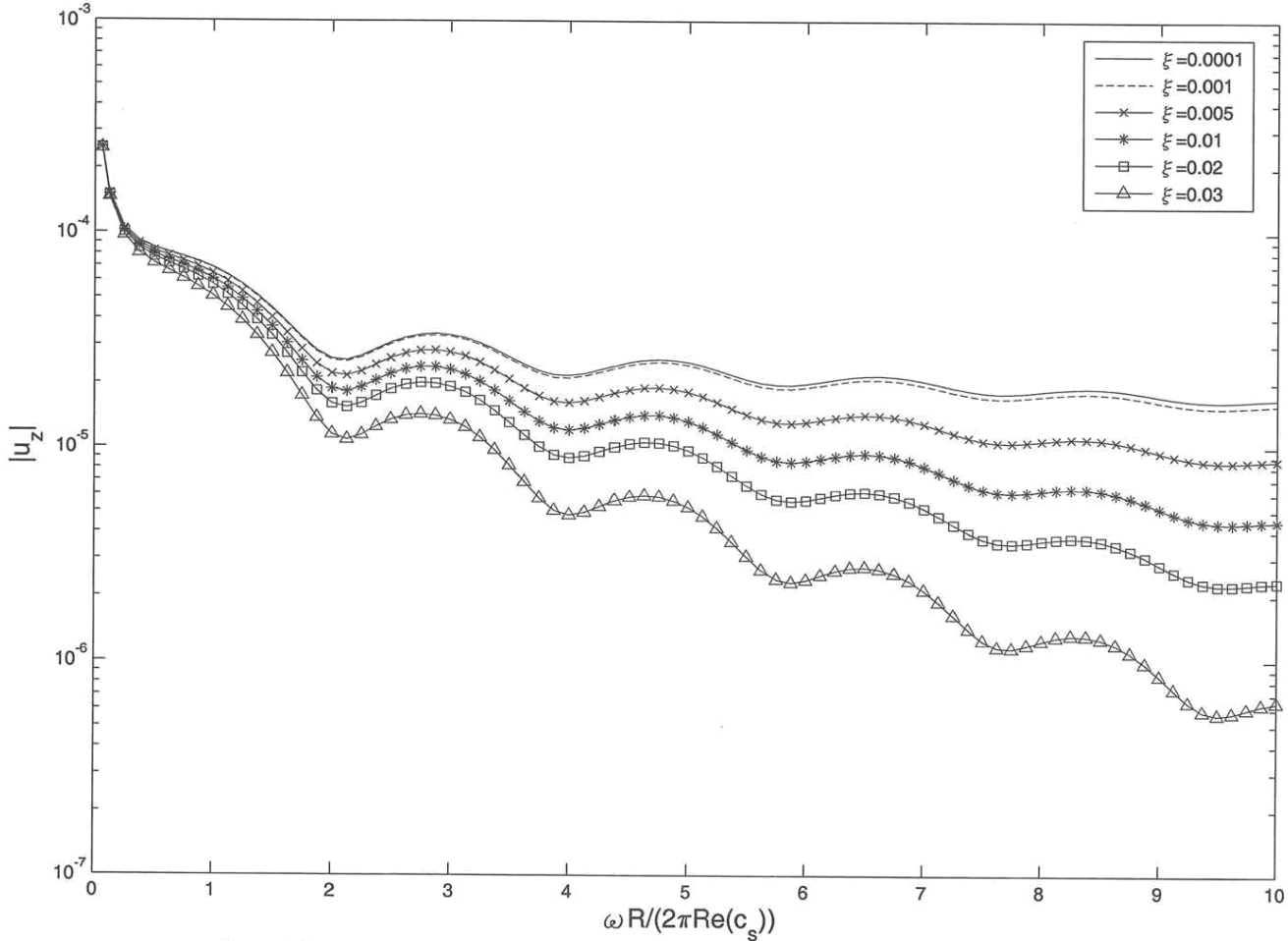

Fig.7: Vibration Amplitude of u_z due to Unit Nondimensional Horizontal Excitation

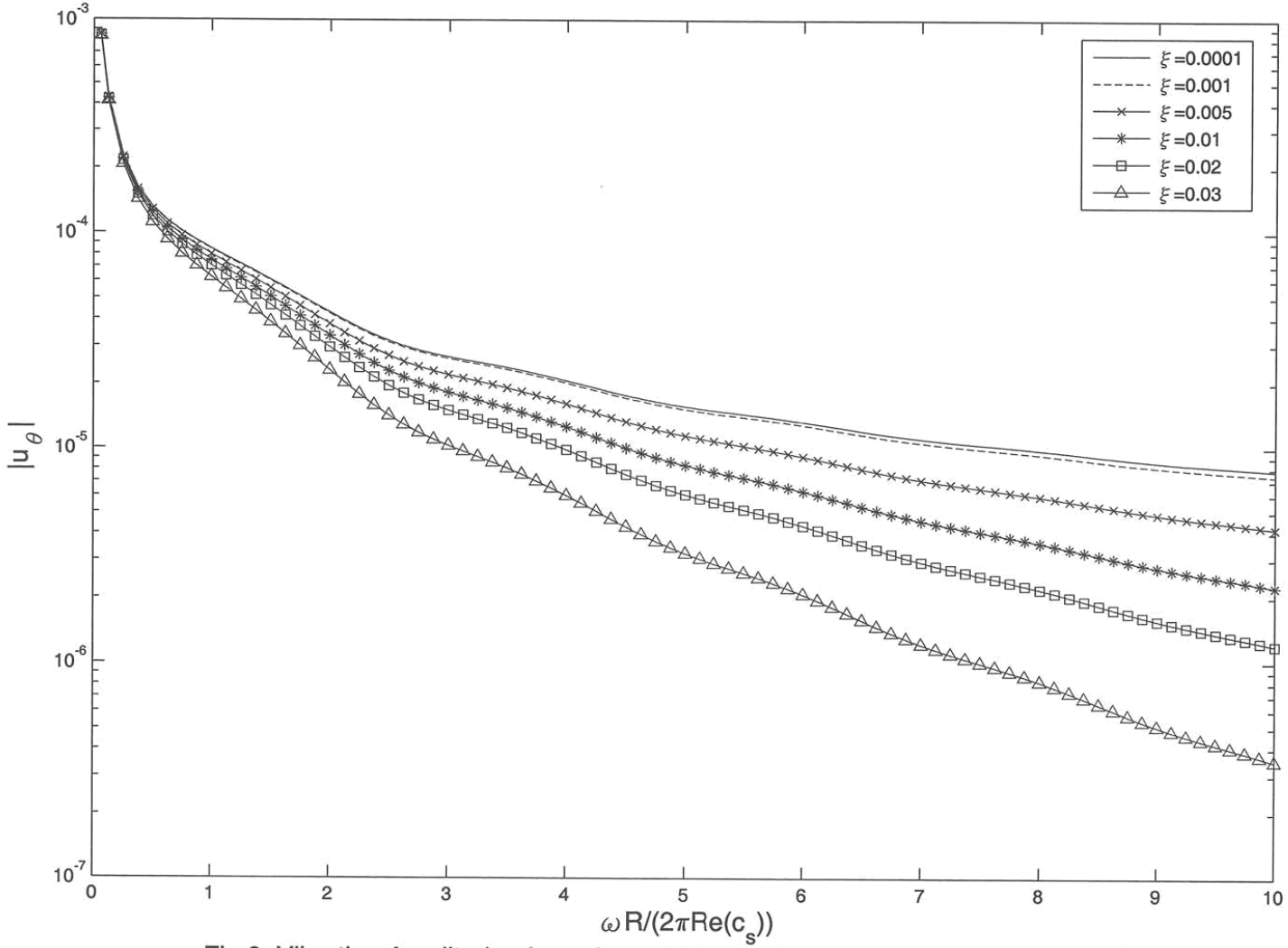

Fig.8: Vibration Amplitude of u_θ due to Unit Nondimensional Horizontal Excitation

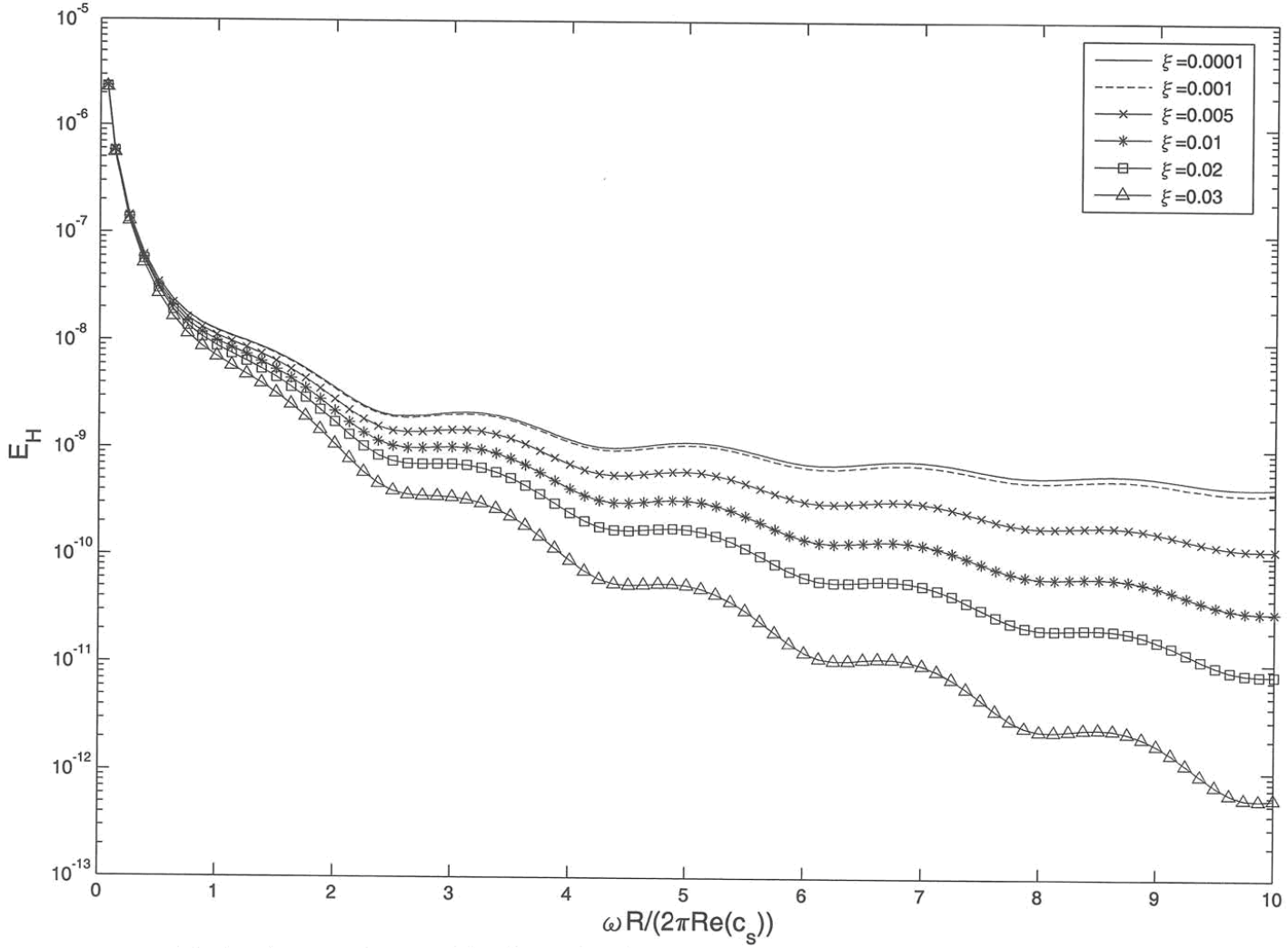

Fig.9: Average Energy Flux Intensity due to Unit Nondimensional Horizontal Excitation

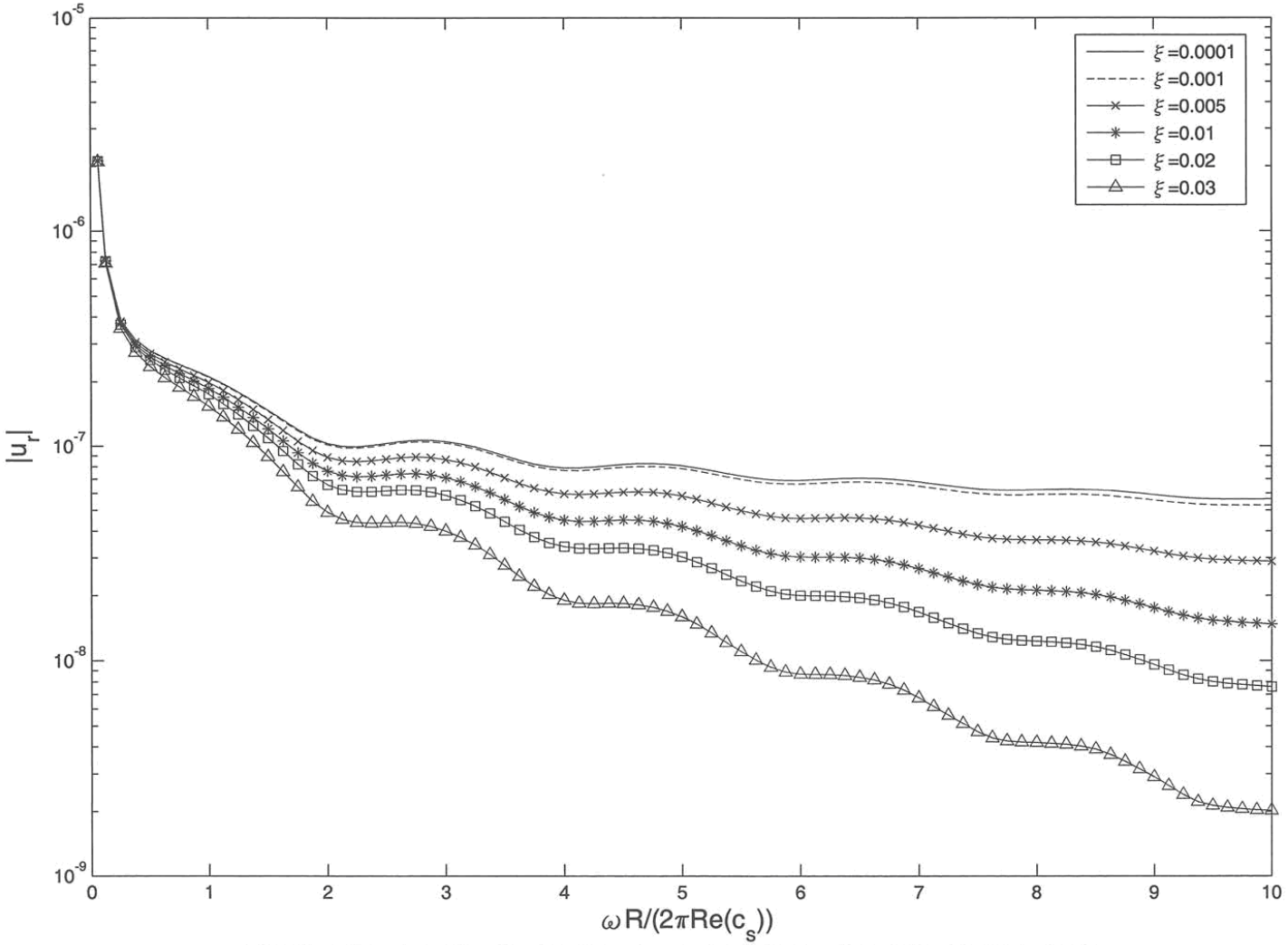

Fig.10: Vibration Amplitude of u_r due to Unit Normalized Rocking Excitation

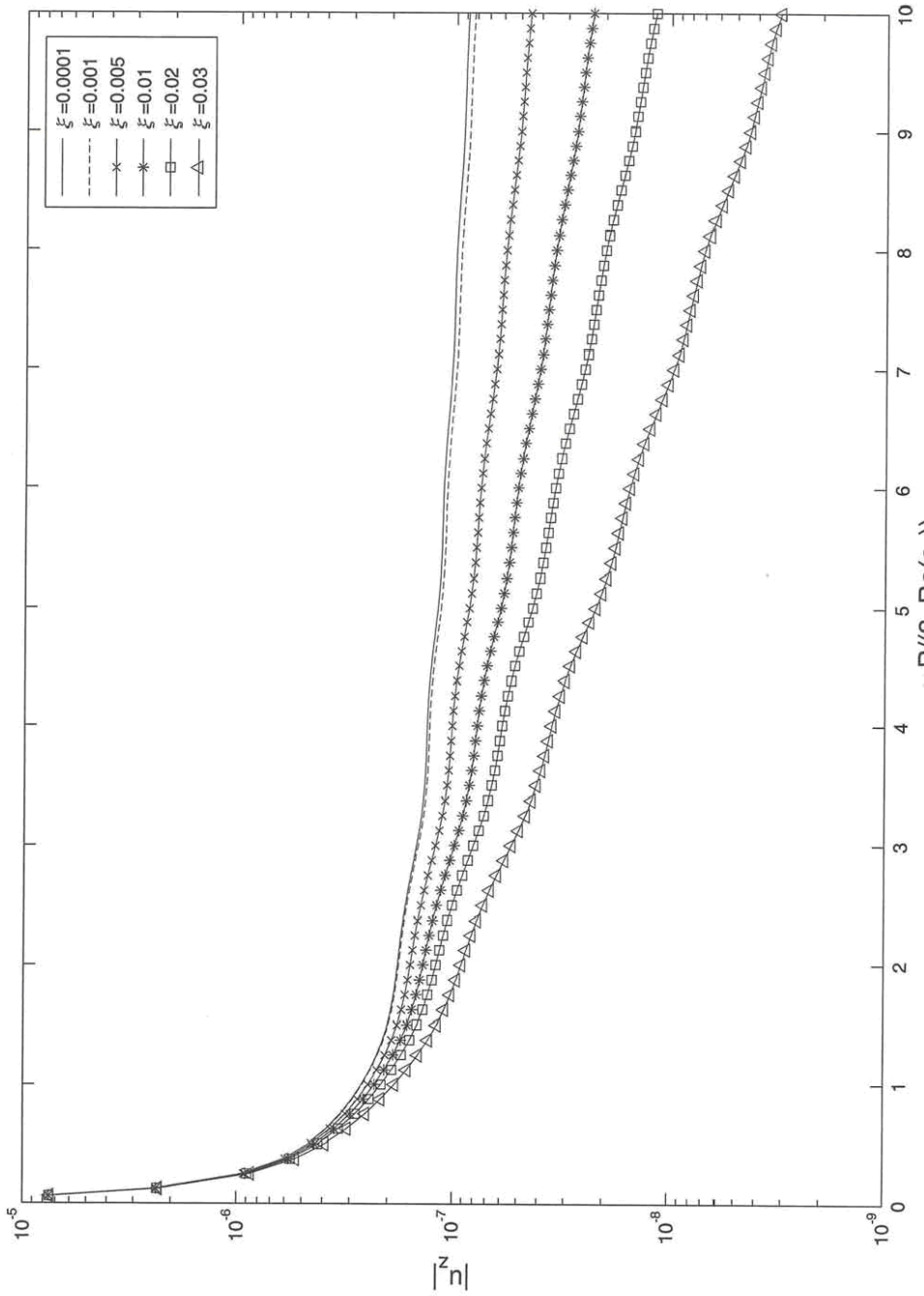

Fig.11: Vibration Amplitude of u_z due to Unit Normalized Rocking Excitation

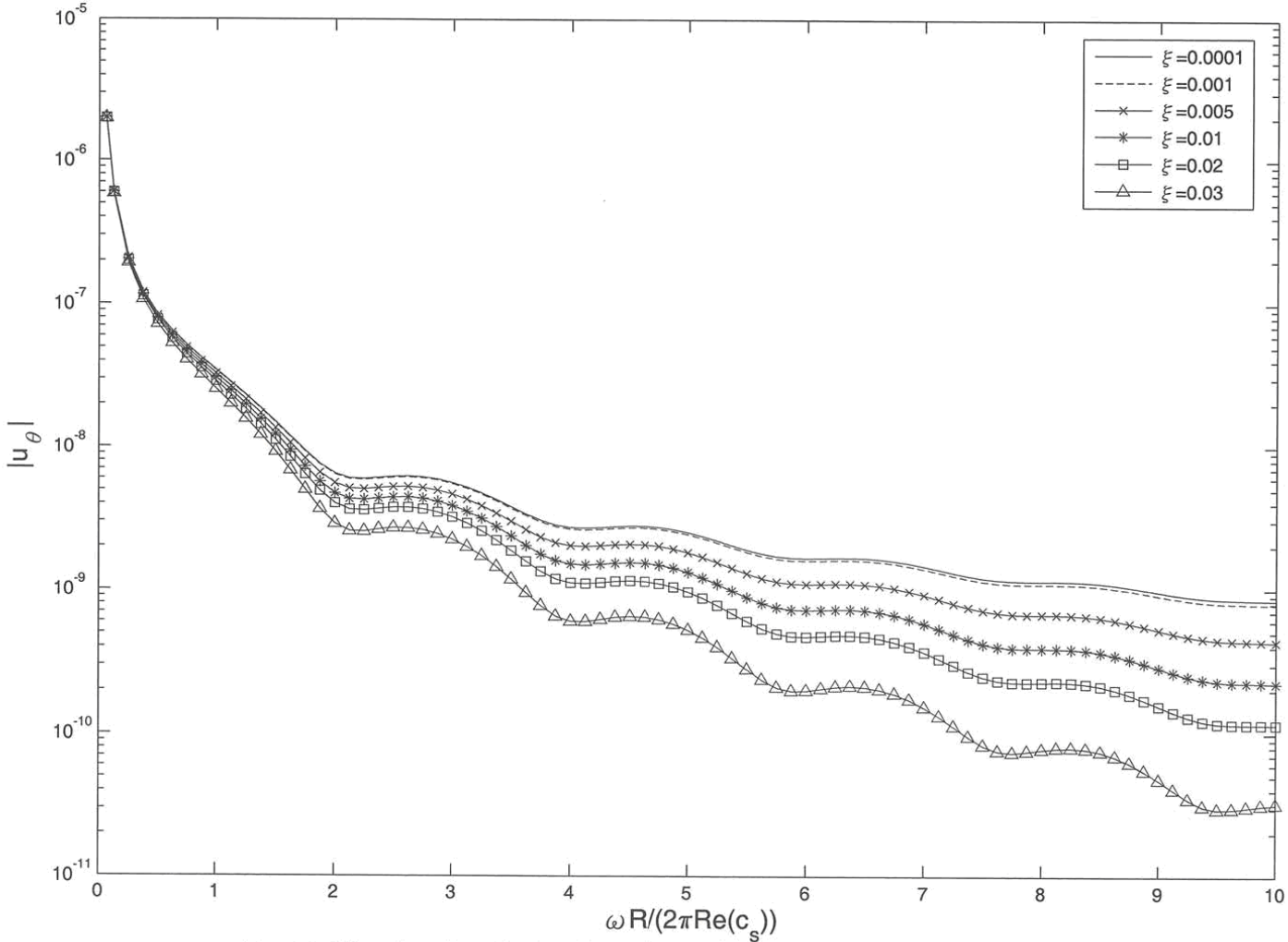

Fig.12: Vibration Amplitude of u_θ due to Unit Normalized Rocking Excitation

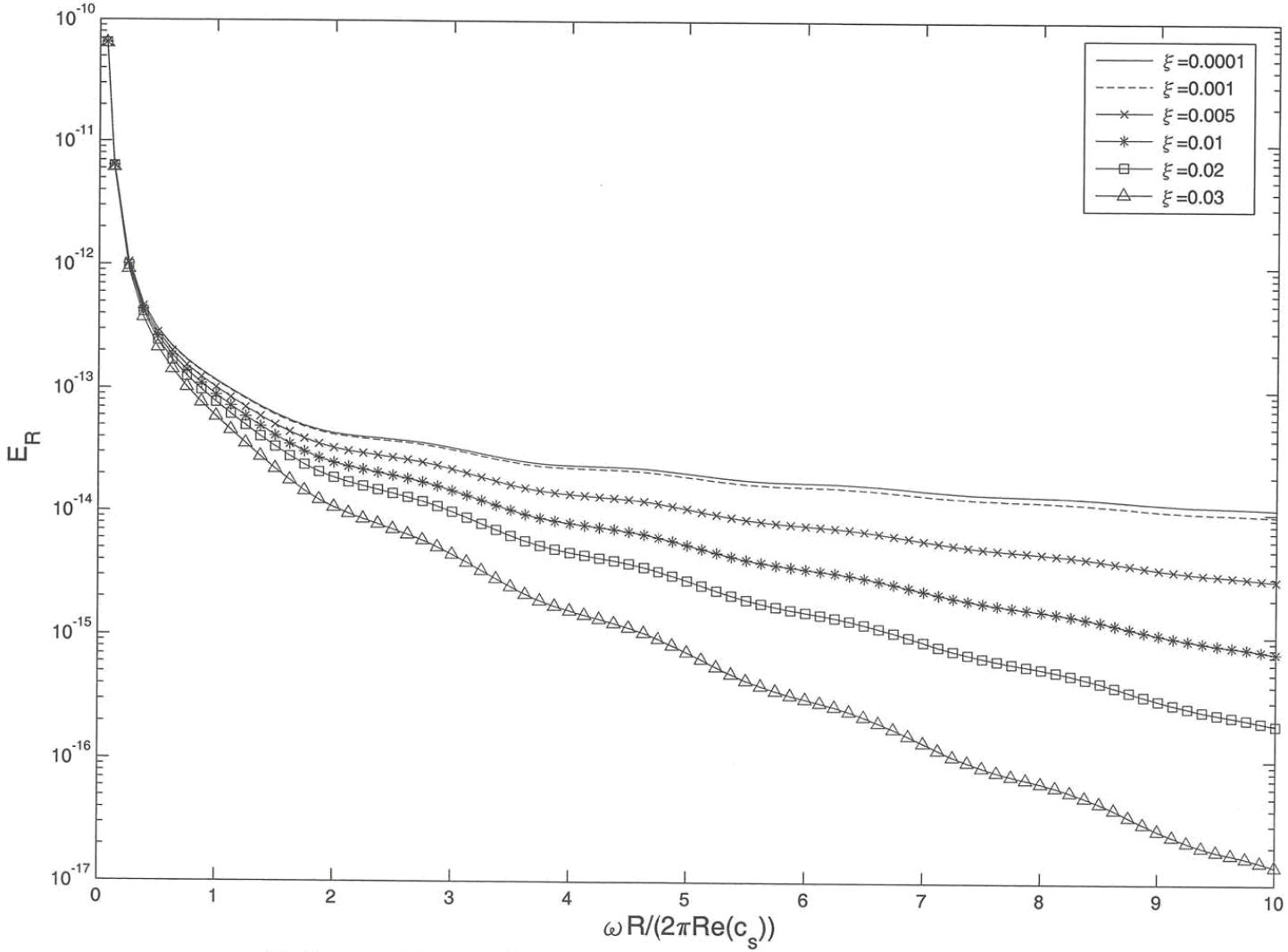

Fig.13: Average Energy Flux Intensity due to Unit Normalized Rocking Excitation

計畫成果自評

本計劃總時程為二年期計畫(96 年 8 月至 98 年 7 月)，本報告為第一年之成果，其計畫成果與預期相符，本計劃總共將可發表一篇國際會議論文，及兩篇國際期刊論文，目前已有一篇在審查中。本計劃所完成之程式包含求得基礎振動或半空間土壤任何位置之振動。本程式將可實際應用在求得某一結構(如高鐵橋梁)之振動對附近結構(高科技廠房)物之影響。

本程式及其理論推導將可擴大求任意基礎形狀及基礎剛度之結構物振動時任何距離之振動大小。